

# Global nitrous oxide production determined by oxygen sensitivity of nitrification and denitrification

**Qixing Ji<sup>1†</sup>, Erik Buitenhuis<sup>2</sup>, Parvadha Suntharalingam<sup>2</sup>, Jorge L. Sarmiento<sup>3</sup> and Bess B. Ward<sup>1</sup>**

<sup>1</sup>Department of Geosciences, Guyot Hall, Princeton University, Princeton, New Jersey, 08540, United States of America.

<sup>2</sup>School of Environmental Science, University of East Anglia, Norwich Research Park, Norwich, Norfolk, NR4 7TJ, United Kingdom.

<sup>3</sup>Program in Atmospheric and Oceanic Sciences, Princeton University, Princeton, New Jersey, 08540, United States of America.

Corresponding author: Qixing Ji ([qji@alumni.princeton.edu](mailto:qji@alumni.princeton.edu))

† Current address: Helmholtz Centre for Ocean Research Kiel, Düsternbrooker Weg 20, 24105, Kiel, Germany.

## Key Points:

- New quantitative relationships between oxygen and nitrous oxide production are derived from direct measurements in low oxygen oceans
- The presence of oxygen reduces nitrous oxide production via nitrification and denitrification
- The latest biogeochemical model incorporating the field measurements and relationships provides new estimate of global marine nitrous oxide flux

This article has been accepted for publication and undergone full peer review but has not been through the copyediting, typesetting, pagination and proofreading process which may lead to differences between this version and the Version of Record. Please cite this article as doi: 10.1029/2018GB005887

## Abstract

The ocean is estimated to contribute up to ~20% of global fluxes of atmospheric nitrous oxide ( $\text{N}_2\text{O}$ ), an important greenhouse gas and ozone depletion agent. Marine oxygen minimum zones (OMZs) contribute disproportionately to this flux. To further understand the partition of nitrification and denitrification and their environmental controls on marine  $\text{N}_2\text{O}$  fluxes, we report new relationships between oxygen concentration and rates of  $\text{N}_2\text{O}$  production from nitrification and denitrification directly measured with  $^{15}\text{N}$  tracers in the Eastern Tropical Pacific. Highest  $\text{N}_2\text{O}$  production rates occurred near the oxic-anoxic interface, where there is strong potential for  $\text{N}_2\text{O}$  efflux to the atmosphere. The dominant  $\text{N}_2\text{O}$  source in OMZs was nitrate reduction, the rates of which were one to two orders of magnitude higher than those of ammonium oxidation. The presence of oxygen significantly inhibited the production of  $\text{N}_2\text{O}$  from both nitrification and denitrification. These experimental data provide new constraints to a multi-component global ocean biogeochemical model, which yielded annual oceanic  $\text{N}_2\text{O}$  efflux of 1.7 – 4.4 Tg-N (median 2.8 Tg-N, 1 Tg =  $10^{12}$  g), with denitrification contributing 20% to the oceanic flux. Thus, denitrification should be viewed as a net  $\text{N}_2\text{O}$  production pathway in the marine environment.

## 1 Introduction

The unprecedented rate of increase in atmospheric nitrous oxide ( $\text{N}_2\text{O}$ ) concentration since the Industrial Revolution (Blasing, 2016) is alarming because  $\text{N}_2\text{O}$  is a strong greenhouse gas and, following the successful mitigation of halocarbons, will be the most important ozone depletion agent by the end of the 21<sup>st</sup> century (Ravishankara *et al.*, 2009).  $\text{N}_2\text{O}$  from soil, coastal waters and the open ocean is emitted into the troposphere, where  $\text{N}_2\text{O}$  is chemically inert, resulting in the pronounced increase of  $\text{N}_2\text{O}$  burden. The average lifetime of  $\text{N}_2\text{O}$  in the atmosphere is estimated to be more than 100 years (Prather *et al.*, 2012); photolytic destruction in the stratosphere is the major sink. Intense  $\text{N}_2\text{O}$  emissions in the open ocean occur in upwelling regions where oxygen minimum zones (OMZs) are located (Codispoti, 2010). OMZs are characterized by sharp oxygen ( $\text{O}_2$ ) gradients (oxycline strength  $>2.5 \mu\text{mol L}^{-1} \text{ m}^{-1}$ ) overlying an anoxic layer of hundreds of meters in depth. Extreme  $\text{N}_2\text{O}$  supersaturation with respect to the atmosphere occurs in the oxycline, indicating active  $\text{N}_2\text{O}$  production and the potential for efflux to the atmosphere (Elkins *et al.*, 1978; Codispoti and Christensen, 1985; Law and Owens, 1990). Although the OMZs occupy

< 1% of the ocean volume (Codispoti *et al.*, 2001), they potentially contribute up to 50% of marine N<sub>2</sub>O efflux (Codispoti, 2010). The Intergovernmental Panel on Climate Change (IPCC) reports that the ocean contributes 3.8 Tg-N yr<sup>-1</sup> (1 Tg = 10<sup>12</sup> g), ~ 21 % of the total N<sub>2</sub>O emissions (Caias *et al.*, 2013). However, incomplete understanding of marine N<sub>2</sub>O production pathways and their sensitivities to environmental factors resulted in large uncertainties of current N<sub>2</sub>O emission estimates (1.8 – 9.4 Tg-N yr<sup>-1</sup>), and limited our ability to predict future N<sub>2</sub>O emission under the changing ocean and climate (Landolfi *et al.*, 2017; Battaglia and Joos, 2018).

Biological N<sub>2</sub>O production in the ocean is attributed to ammonium (NH<sub>4</sub><sup>+</sup>) oxidation, nitrite (NO<sub>2</sub><sup>-</sup>) reduction and nitrate (NO<sub>3</sub><sup>-</sup>) reduction (Figure 1). During aerobic NH<sub>4</sub><sup>+</sup> oxidation to NO<sub>2</sub><sup>-</sup>, the first step in nitrification (by both bacteria and archaea), N<sub>2</sub>O is emitted as a byproduct, with higher N<sub>2</sub>O yield (the molar nitrogen ratio of N<sub>2</sub>O to NO<sub>2</sub><sup>-</sup> production) at lower O<sub>2</sub> conditions (Goreau *et al.*, 1980; Löscher *et al.*, 2012). Under low O<sub>2</sub> and anoxic conditions, NO<sub>3</sub><sup>-</sup> and NO<sub>2</sub><sup>-</sup> can be reduced to N<sub>2</sub>O through stepwise conventional denitrification (NO<sub>3</sub><sup>-</sup> → NO<sub>2</sub><sup>-</sup> → NO → N<sub>2</sub>O), with organic matter as the electron donor. Nitrite reduction, which occurs in O<sub>2</sub> conditions from fully saturated to functional anoxia (Frame and Casciotti, 2010), is mediated by both nitrifiers (Poth and Focht, 1985) and denitrifiers (Cohen and Gordon, 1978). ‘Nitrifier denitrification’ refers to NO<sub>2</sub><sup>-</sup> reduction to N<sub>2</sub>O in oxygenated water column where conventional denitrification is insignificant (Wilson *et al.*, 2014). In the OMZs, the sharp O<sub>2</sub> gradient provides niches for both nitrifying and denitrifying organisms to enable N<sub>2</sub>O production from both nitrification and denitrification (Codispoti and Christensen, 1985). In this study, ‘nitrification’ refers to NH<sub>4</sub><sup>+</sup> oxidation whereas ‘denitrification’ refers to NO<sub>3</sub><sup>-</sup> and NO<sub>2</sub><sup>-</sup> reduction. At present, distinguishing nitrifier denitrification from conventional denitrification (i.e. both can conduct

$\text{NO}_2^-$  reduction to  $\text{N}_2\text{O}$ ) in natural environments is difficult due to the lack of reliable methodology.

Nitrification is regarded as the main pathway of global oceanic  $\text{N}_2\text{O}$  production because denitrification is mainly restricted to OMZs and because  $\text{N}_2\text{O}$  consumption is assumed to dominate over  $\text{N}_2\text{O}$  production by denitrification in the OMZs (Codispoti, 2010; Freing *et al.*, 2012). This notion was challenged by recent observations and model analysis (Babbin *et al.*, 2015; Ji *et al.*, 2015; Bourbonnais *et al.*, 2017), which suggested high rates of  $\text{N}_2\text{O}$  production from  $\text{NO}_3^-$  reduction in the OMZs. Lacking reliable quantification of nitrogen cycling processes in OMZs, previous biogeochemical models predominantly employed simple parameterizations representing  $\text{N}_2\text{O}$  production derived from limited culture analyses and in-situ measurements, and model analysis of the relative contribution of  $\text{N}_2\text{O}$  production from denitrification and nitrification to the total oceanic flux is uncertain (Suntharalingam *et al.*, 2012; Battaglia and Joos, 2018).

We applied nitrogen stable isotope ( $^{15}\text{N}$ ) incubation experiments to directly measure rates and pathways of  $\text{N}_2\text{O}$  production in the OMZs of the Eastern Tropical South and North Pacific (ETSP and ETNP). To evaluate control of  $\text{N}_2\text{O}$  production by oxygen, we derived quantitative relationships between oxygen concentration and  $\text{N}_2\text{O}$  production from  $\text{NH}_4^+$  oxidation,  $\text{NO}_2^-$  and  $\text{NO}_3^-$  reduction. The rate distribution and  $\text{O}_2$  relationships were incorporated into a multi-component ocean biogeochemistry and ecosystem model to estimate global oceanic  $\text{N}_2\text{O}$  fluxes, and to partition the contributions of the nitrification and denitrification pathways.

## 2 Methods

### 2.1 Shipboard Sampling

Shipboard sampling and incubation experiments were carried out on the *R/V Atlantis* during January, 2015 (Cruise ID: AT26-26); and *R/V Ronald H. Brown* during April 2016 (Cruise ID: RB1603). Samples were collected from the North (15°N – 20°N) and South Pacific (10°S – 20°S) coastal upwelling zones off the coast of Mexico and Peru (Figure 2). Stations were chosen to represent coastal environment (<100 nautical miles from the coast) and open-ocean environment (>200 nautical miles from the coast). Water was collected in 12 L Niskin bottles mounted on a standard conductivity-temperature-depth (CTD) rosette system. During the 2015 cruise, an oxygen sensor (Seabird SBE43, Bellevue, WA) calibrated by Winkler titration (detection limit 0.7 – 2.5  $\mu\text{mol kg}^{-1}$ ), and a real-time STOX sensor (detection limit 10 nmol  $\text{L}^{-1}$  (Revsbech *et al.*, 2009)) were deployed on the CTD. During the 2016 cruise, only the Seabird oxygen sensor was deployed. Dissolved inorganic nitrogen species ( $\text{NH}_4^+$ ,  $\text{NO}_2^-$  and  $\text{NO}_3^-$ ) were measured onboard:  $\text{NH}_4^+$  was measured fluorometrically by reaction with orthophthaldialdehyde (OPA) (Holmes *et al.*, 1999);  $\text{NO}_2^-$  was measured using a colorimetric method (Hansen and Koroleff, 1999) and  $\text{NO}_3^- + \text{NO}_2^-$  was measured using cadmium reduction protocols established by UNESCO (UNESCO, 1994). See Figure S1 for typical profiles of oxygen and inorganic nitrogen during ETSP 2015 and ETNP 2016. Physical and chemical data from the ETSP in 2013 were described previously (Ji *et al.*, 2015).

### 2.2 $\text{N}_2\text{O}$ production rate measurements

Incubation experiments to measure  $\text{N}_2\text{O}$  production using  $^{15}\text{N}$  tracers were targeted at depths with water column features including the surface mixed layer, the base of the euphotic layer, local  $[\text{NO}_2^-]$  maxima, sharp oxygen gradients (oxycline) and oxic-anoxic interfaces. Seawater was sampled from 12 L Niskin bottles into the bottom of acid washed, 60-mL glass serum bottles (Catalog# 223745, Wheaton, USA) and then allowed to overflow two to three

times the volume before sealing the bottles with butyl septa and aluminum rings. To facilitate tracer addition, as well as compensating for oxygen contamination from air, helium headspace (3 mL) was created. Three suites of  $^{15}\text{N}$  tracer solutions ( $^{15}\text{NH}_4^+$  plus  $^{14}\text{NO}_2^-$ ,  $^{15}\text{NO}_2^-$  plus  $^{14}\text{NH}_4^+$ ,  $^{15}\text{NO}_3^-$  plus  $^{14}\text{NH}_4^-$  and  $^{14}\text{NO}_2^-$ ) were applied to enrich  $^{15}\text{NH}_4^+$ ,  $^{15}\text{NO}_2^-$  and  $^{15}\text{NO}_3^-$  to 0.2, 0.4 and 0.4  $\mu\text{mol L}^{-1}$  (final concentration), respectively; and increase concentrations of  $^{14}\text{NH}_4^+$ ,  $^{14}\text{NO}_2^-$  or  $^{14}\text{NO}_3^-$  by 0.2, 0.4 and 0.4  $\mu\text{mol L}^{-1}$  ( $\mu\text{M}$ ), respectively. Most of the samples had *in situ* concentrations of  $\text{NH}_4^+$  below 0.02  $\mu\text{M}$  (Figure S1) and thus rates of  $\text{N}_2\text{O}$  and  $\text{NO}_2^-$  production from  $\text{NH}_4^+$  should be treated as potential rates. Samples for incubation experiments, except for one surface sample (10 m), had *in situ*  $\text{NO}_3^-$  concentrations  $> 4.6 \mu\text{M}$ ; samples collected from the ODZ and outside the ODZ generally had *in situ*  $\text{NO}_2^-$  concentrations  $> 1 \mu\text{M}$  and  $< 0.1 \mu\text{M}$ , respectively (see supplementary dataset). Tracer solutions were made from deionized water, and were flushed with helium gas before adding 0.1mL into each sample. Incubations lasted 12 – 18 hours in temperature-controlled chambers ( $\pm 2^\circ\text{C}$  of *in situ* temperature), during which duplicate samples were preserved every 6 – 9 hours (3 time points in total) with 0.1 mL saturated mercuric chloride ( $\text{HgCl}_2$ ). Dilution of  $^{15}\text{N}$ -labeled species were considered insignificant due to short incubation time.

The effect of oxygen concentrations on  $\text{N}_2\text{O}$  production was further investigated in the top of the anoxic layer (*in situ*  $[\text{O}_2] < 0.1 \mu\text{M}$  verified by STOX sensor). During the 2015 ETSP cruise, the depths were 160 m and 80 m at offshore and coastal stations, respectively. During the 2016 ETNP cruise, the interface was at 188 m and 89 m at offshore and coastal stations, respectively. Samples were acquired using a pump profiling system (PPS) equipped with a CTD package, an oxygen sensor (SBE-25, Seabird Electronics, Bellevue, WA), and a real-time STOX unit. The PPS minimized oxygen contamination during sampling and allowed better representation of *in situ* anoxic conditions during incubation experiments. The

serum bottles were filled directly from the pump outlet and sealed without a headspace with septa and aluminum rings. Then, 3.2, 3.5, 4.0, 5.0, 8.0 mL helium headspace was created, volumes of 0.2, 0.5, 1.0, 2.0 and 5.0 mL of O<sub>2</sub> saturated site water (~225 µM) were injected into the incubation bottles to attain 0.3, 0.7, 1.4, 2.8 and 7 µM dissolved [O<sub>2</sub>] (calculated by assuming equilibrium between the water phase and 3.0 mL final headspace in the incubation bottles (Garcia and Gordon, 1992). The same suite of tracers as above was utilized. Incubation lasted 12 – 18 hours at ±2 °C of *in situ* temperatures, during which duplicate samples were preserved every 6 – 9 hours (3 time points in total) with 0.1 mL saturated HgCl<sub>2</sub>.

Upon return to the home laboratory, N<sub>2</sub>O in the water and headspace was stripped from the samples and analyzed using an autosampler in line with a cryo-focusing unit with helium as carrier gas, and injected into a Thermo-Finnigan Delta V for N<sub>2</sub>O concentration and isotope ratio (m/z = 44, 45, 46) measurements. N<sub>2</sub>O concentration was calculated from the amount of N<sub>2</sub>O detected by mass spectrometry divided by the volume of seawater in the serum bottles (calibrated as 56.5 ± 0.1 mL). N<sub>2</sub>O production was calculated from the progressive increase in mass 45 and 46 N<sub>2</sub>O (<sup>45</sup>N<sub>2</sub>O and <sup>46</sup>N<sub>2</sub>O) in time course experiments.

Equation (1)

$$R = \frac{1}{F} \times \left( \frac{d^{45}\text{N}_2\text{O}}{dt} + 2 \times \frac{d^{46}\text{N}_2\text{O}}{dt} \right)$$

where  $d^{45}\text{N}_2\text{O}/dt$  and  $d^{46}\text{N}_2\text{O}/dt$  represent the production rates of during incubation of <sup>45</sup>N<sub>2</sub>O and <sup>46</sup>N<sub>2</sub>O. F represents the <sup>15</sup>N atom fraction in the initial substrate pool (NH<sub>4</sub><sup>+</sup>, NO<sub>2</sub><sup>-</sup>, and NO<sub>3</sub><sup>-</sup>). Rates were considered significant if the linear regression of the time course data having p<0.05 (n=5, ANOVA).

### 2.3 NO<sub>2</sub><sup>-</sup> production measurements

After samples were analyzed for N<sub>2</sub>O production, samples spiked with <sup>15</sup>NH<sub>4</sub><sup>+</sup> were also assayed for <sup>15</sup>NO<sub>2</sub><sup>-</sup> to determine N<sub>2</sub>O yield during nitrification. 3 mL of each sample was

transferred using a 5-mL gas-tight glass syringe (Hamilton Co., Reno, NV, USA) from the 60-mL serum bottle to a helium-flushed 20-mL glass vial (Catalog# C4020-25, Thermo Fisher Scientific, Waltham, MA). Dissolved  $^{15}\text{NO}_2^-$  was converted to N<sub>2</sub>O using the acetic acid-treated sodium azide solution for quantitative conversion (McIlvin and Altabet, 2005). Resulting N<sub>2</sub>O was measured on the Thermo-Finnigan Delta V for isotope ratio measurements.

#### 2.4 Data Analysis

All data were deposited in Microsoft Excel® for statistical analysis and figure production. Oxygen profiles (1 meter binned-average from the CTD data package) were computed as the 5 meter moving average. The depth of the oxic-anoxic interface was determined as the depth below the oxycline at which the standard deviation of the moving-averaged oxygen concentrations became  $< 0.1 \mu\text{mol kg}^{-1}$ .

#### 2.5 Three-dimensional marine N<sub>2</sub>O production simulation

The prognostic global ocean general circulation Nucleus for European Modelling of the Ocean (NEMO) v3.1 model (Madec *et al.*, 1998) was forced by daily meteorological data from the National Centers for Environmental Prediction (NCEP) reanalysis. Embedded in the ocean circulation model, biogeochemistry was simulated by the PlankTOM10 model (Le Quéré *et al.*, 2016; Buitenhuis *et al.*, 2018). The NEMO-PlankTOM10 system has a horizontal resolution of 2° with higher resolution (up to 0.5°) in tropical and polar latitudes. There are 31 vertical levels in the entire water column and 10 m resolution in the upper 100 m. The oxygen distribution in the ocean was fixed according to the reanalysis of the World Ocean Atlas oxygen dataset, which had minimum [O<sub>2</sub>] > 1 μM (Bianchi *et al.*, 2012). The export production was estimated to be 5.8 PgC yr<sup>-1</sup>, consistent with recent model estimates (Siegel *et al.*, 2014; Bisson *et al.*, 2018). The NEMO-PlankTOM10 system

simulates the rates of nitrogen remineralization and N<sub>2</sub>O production by relating oxygen consumption and organic matter remineralization below the euphotic zone:

**Equation (2)**

[Oxygen Consumption Rate] = respiration by the 10 model plankton functional types (6 phytoplankton, 3 zooplankton and picoheterotrophs (*Bacteria + Archaea*))

**Equation (3)**

[Nitrogen remineralization rate] = [Oxygen Consumption Rate] × (16 mol N / 172 mol O<sub>2</sub>) (Takahashi *et al.*, 1985)

Parameterization of N<sub>2</sub>O production was modified from previous model setup (Suntharalingam *et al.*, 2012; Capelle *et al.*, 2018) so as to employ *in situ* oxygen concentrations to compute N<sub>2</sub>O production from nitrification and denitrification:

**Equation (4)**

$$\text{N}_2\text{O Source} = J_1 + J_2$$

$$J_1 = [a / [\text{O}_2] (\mu\text{M}) + b] \times 0.01 \times [\text{Nitrogen remineralization rate}]$$

$$J_2 = \beta \times f(\text{O}_2) \times [\text{Nitrogen remineralization rate}]$$

The two separate terms ( $J_1$  and  $J_2$ ) represent (a) NH<sub>4</sub><sup>+</sup> oxidation to N<sub>2</sub>O in the presence of oxygen ( $J_1$ ), which is parameterized according to an empirical relationship between N<sub>2</sub>O yield and *in situ* O<sub>2</sub> concentrations during NH<sub>4</sub><sup>+</sup> oxidation (see section 3.1 and Figure 4); and (b) the enhanced N<sub>2</sub>O production via NO<sub>2</sub><sup>-</sup> and NO<sub>3</sub><sup>-</sup> reduction in OMZs ( $J_2$ ). The linear scaling parameter  $\beta$  is derived from Suntharalingam *et al.* (2012), which represents increased N<sub>2</sub>O production from denitrification in suboxic conditions; and is set at 0.215, meaning up to 0.215 mol N<sub>2</sub>O-N is produced when 1 mol of nitrogen is remineralized. The function  $f(\text{O}_2)$  accounts for the functional dependence of N<sub>2</sub>O yield on oxygen level.

**Equation (5)**

$$f(\text{O}_2) = \exp(\lambda ([\text{O}_2] - [\text{O}_{2\text{-offset}}])) \text{ when } [\text{O}_2] > [\text{O}_{2\text{-offset}}]$$

$$f(\text{O}_2) = [\text{O}_2] / [\text{O}_{2\text{-offset}}] \text{ when } [\text{O}_2] < [\text{O}_{2\text{-offset}}]$$

The  $[\text{O}_{2\text{-offset}}]$  represents the oxygen concentration below which net N<sub>2</sub>O production is reduced due to N<sub>2</sub>O consumption by denitrification, and is set to 1 μM (Dalsgaard *et al.*,

2014; Capelle *et al.*, 2018). The effect of O<sub>2</sub> on N<sub>2</sub>O production from denitrification (NO<sub>2</sub><sup>-</sup> and NO<sub>3</sub><sup>-</sup> reduction) was experimentally measured (see section 3.2) to determine the parameterization of  $\lambda$  (see section 3.3 and Table 1).

The evolution of the atmospheric N<sub>2</sub>O partial pressure since the Industrial Revolution is parameterized as:

$$\text{Equation (6)} \quad pN_2O_{\text{atm}} = 0.000009471353 \times Y^3 - 0.05214714 \times Y^2 + 95.68066 \times Y - 58228.41$$

in which  $pN_2O_{\text{atm}}$  is in natm and  $Y$  is the decimal year (Buitenhuis *et al.*, 2018, as corrected from (Freing *et al.*, 2009). Oceanic N<sub>2</sub>O flux to the atmosphere ( $F$ ) is computed as the product of gas transfer velocity ( $k$ ) and the difference between model-derived surface ocean concentration ( $C_s$ ) and equilibrium concentration ( $C_{\text{eq}}$ ):

$$\text{Equation (7)} \quad F = k \times (C_s - C_{\text{eq}})$$

The  $C_{\text{eq}}$  is computed following the equations of N<sub>2</sub>O solubility in seawater with in situ temperature, salinity and  $pN_2O_{\text{atm}}$  (Weiss and Price, 1980). Daily NCEP wind product ( $U$ ) and Schmidt number for N<sub>2</sub>O ( $Sc$ ) is used to calculate the gas transfer velocity  $k$  (Wanninkhof, 1992).

$$\text{Equation (8)} \quad k = 0.31U^2 (Sc/660)^{-0.5}$$

Model spin-up was performed to reach steady state of N<sub>2</sub>O concentration. Thus water column N<sub>2</sub>O production approximated to the oceanic flux. Statistical comparison of simulated N<sub>2</sub>O distribution pattern both at the surface and depth were performed (Figure S2) with respect to observations compiled in the MEMENTO database (Kock and Bange, 2015).

### 3 Results

Rates of N<sub>2</sub>O production from NH<sub>4</sub><sup>+</sup> oxidation (Figure 3A), NO<sub>2</sub><sup>-</sup> reduction (Figure 3B) and NO<sub>3</sub><sup>-</sup> reduction (Figure 3C) were relatively higher across the oxic-anoxic interface compared to depths > 100 m deeper or shallower than the interface in the Eastern North and South Pacific OMZs. Highest rates of N<sub>2</sub>O production from NH<sub>4</sub><sup>+</sup> oxidation, NO<sub>2</sub><sup>-</sup> and NO<sub>3</sub><sup>-</sup> reduction were detected close to ( $\pm$  50 m) the oxic-anoxic interface. Rates were very low at depths  $\geq$  200 m below the oxic-anoxic interface and in the oxygenated layer  $\geq$  100 m above the interface. The rates of N<sub>2</sub>O production from nitrification and denitrification, and their control by environmental factors are presented below.

#### 3.1 N<sub>2</sub>O production in the OMZs

For N<sub>2</sub>O production from NH<sub>4</sub><sup>+</sup> oxidation, maximum rates (up to 0.05 nmol-N L<sup>-1</sup> d<sup>-1</sup>) were detected within 100 m above the oxic-anoxic interface (Figure 3A). This depth range within 100 m above the interface generally corresponds to the oxycline and N<sub>2</sub>O supersaturation (data not shown). In the oxygenated layer, the majority of the rate measurements were 0 – 0.02 nmol-N L<sup>-1</sup> d<sup>-1</sup>, and the rates decreased at shallower depths. In the anoxic layer below the interface, NH<sub>4</sub><sup>+</sup> oxidation is inhibited by anoxia, resulting in very low or undetectable rates of N<sub>2</sub>O production from NH<sub>4</sub><sup>+</sup> oxidation. At deeper depths ( $\geq$  200 m below the oxic-anoxic interface), N<sub>2</sub>O production rates from NH<sub>4</sub><sup>+</sup> oxidation were very slow (< 0.001 nmol-N L<sup>-1</sup> d<sup>-1</sup>). Direct measurement of N<sub>2</sub>O yield in natural waters under a range of O<sub>2</sub> conditions (Figure 4) was achieved by the simultaneous measurements of N<sub>2</sub>O and NO<sub>2</sub><sup>-</sup> production from NH<sub>4</sub><sup>+</sup> oxidation. Consistent with elevated rates of N<sub>2</sub>O production from NH<sub>4</sub><sup>+</sup> oxidation close to the oxic-anoxic interface, the N<sub>2</sub>O yield increased non-linearly from 0.003 – 0.06 % at > 50  $\mu$ M O<sub>2</sub>, to higher than 2 % at < 0.5  $\mu$ M O<sub>2</sub>. Particularly at O<sub>2</sub> concentration < 5  $\mu$ M, significant increase of yield up to two orders of magnitude, was observed with decreasing O<sub>2</sub> concentration. An empirical fit between N<sub>2</sub>O yield (%) from nitrification and O<sub>2</sub> concentration ( $\mu$ M) was derived: Yield = (0.2 $\pm$ 0.13) / [O<sub>2</sub>] + (0.08 $\pm$ 0.04),

$r^2 = 0.33$ . This relationship implies that (1) the range of N<sub>2</sub>O yield during nitrification at 0.1 – 300 μM O<sub>2</sub> concentrations is 0.04 – 3 %; (2) outside of the OMZ at > 50 μM O<sub>2</sub>, the uncertainty range of the yield is 0.04 – 0.12 %. Compared to previous studies relying on cultured AOB for yield measurements (Goreau *et al.*, 1980; Nevison *et al.*, 2003), natural waters from the OMZs have 10 – 100 fold lower yield at O<sub>2</sub> concentrations < 10 μM (Figure 4). Within the oxycline where the O<sub>2</sub> concentration generally varies between 10 and 100 μM, the N<sub>2</sub>O yield measurements of natural waters are 2 – 10 fold lower than those from cultured AOB.

N<sub>2</sub>O production from both NO<sub>2</sub><sup>-</sup> and NO<sub>3</sub><sup>-</sup> reduction was detected in the oxycline, generally within 30 m above the oxic-anoxic interface and in the anoxic depths (Figures 3B - C). Highest rates (up to 2 nmol-N L<sup>-1</sup> d<sup>-1</sup>) were detected within the oxycline and were 10 – 100-fold higher than N<sub>2</sub>O production from NH<sub>4</sub><sup>+</sup> oxidation. The majority of rates of NO<sub>2</sub><sup>-</sup> reduction to N<sub>2</sub>O ranged from 0 – 1.5 nmol-N L<sup>-1</sup> d<sup>-1</sup>, except for one measurement of 6.8 nmol-N L<sup>-1</sup> d<sup>-1</sup> (Figure 3B). Highest rates of N<sub>2</sub>O production from NO<sub>2</sub><sup>-</sup> and NO<sub>3</sub><sup>-</sup> reduction occurred just below the oxic-anoxic interface. Both NO<sub>2</sub><sup>-</sup> and NO<sub>3</sub><sup>-</sup> are substrates for denitrifiers producing N<sub>2</sub>O. However, in most paired samples, rates of N<sub>2</sub>O production from NO<sub>3</sub><sup>-</sup> reduction were 2 – 7-fold higher than N<sub>2</sub>O production from NO<sub>2</sub><sup>-</sup> reduction; the median contribution of NO<sub>3</sub><sup>-</sup> reduction to total N<sub>2</sub>O production from denitrification is 73%. The relative magnitude of the two rates may be related to the ratio of NO<sub>2</sub><sup>-</sup> and NO<sub>3</sub><sup>-</sup> concentrations (Figure 5). The linear regressions between the ratio of N<sub>2</sub>O production rates from NO<sub>2</sub><sup>-</sup> vs. from NO<sub>3</sub><sup>-</sup>, and the concentration ratio of [NO<sub>2</sub><sup>-</sup>]/[NO<sub>3</sub><sup>-</sup>] are as follows: Within concentration ratio of 0 – 0.5,  $y = 0.5066x + 0.0137$ ,  $r^2=0.43$ ,  $p = 0.00015$  (ANOVA,  $n=28$ ); within concentration ratio of 0 – 2.0,  $y = 0.3025x + 0.0625$ ,  $r^2=0.896$ ,  $p = 1E-15$  (ANOVA,  $n=30$ ).

### 3.2 Effects of Oxygen on N<sub>2</sub>O production

The effects of elevated O<sub>2</sub> (0 – 7 μM) on N<sub>2</sub>O production from NH<sub>4</sub><sup>+</sup> oxidation, NO<sub>2</sub><sup>-</sup> reduction and NO<sub>3</sub><sup>-</sup> reduction were experimentally investigated at the oxic-anoxic interface in both coastal and offshore waters (Figure 6). Under *in situ* O<sub>2</sub> concentration (< 0.1 μM), coastal stations had higher rates of N<sub>2</sub>O production from NH<sub>4</sub><sup>+</sup> oxidation, NO<sub>2</sub><sup>-</sup> reduction and NO<sub>3</sub><sup>-</sup> reduction. An exception was that, during 2015 ETSP cruise, similar rates of NO<sub>2</sub><sup>-</sup> reduction to N<sub>2</sub>O in coastal and offshore stations were observed (0.45 nmol-N L<sup>-1</sup> d<sup>-1</sup>, Figure 6B). Highest rates of N<sub>2</sub>O production from NH<sub>4</sub><sup>+</sup> and NO<sub>2</sub><sup>-</sup> were measured under *in situ* O<sub>2</sub> concentration. These rates were significantly reduced during the course incubation experiments (within a day) in the presence of > 1 μM O<sub>2</sub>. At 7 μM O<sub>2</sub>, rates of N<sub>2</sub>O production from NH<sub>4</sub><sup>+</sup> and NO<sub>2</sub><sup>-</sup> were reduced by 50 – 100 % (Figures 6A and 6B). The NO<sub>2</sub><sup>-</sup> data were fitted with exponential-type inhibition kinetics [inhibition = 1 – exp (-k × O<sub>2</sub> (μM))] to derive half inhibition O<sub>2</sub> concentration (C<sub>50</sub> = -ln(0.5)/k). The C<sub>50</sub> for NO<sub>2</sub><sup>-</sup> reduction to N<sub>2</sub>O in the ETSP and ETNP at both coastal and offshore stations was 1.5 ± 0.9 μM (p = 0.01). By contrast, increasing O<sub>2</sub> concentration up to 7 μM was ineffective to inhibit N<sub>2</sub>O production from NO<sub>3</sub><sup>-</sup> reduction during the 18-hour long incubations (Figure 6C). At the coastal and offshore stations, the range of rates was 0.8 – 1.2 nmol-N L<sup>-1</sup> d<sup>-1</sup> and 0 – 0.13 nmol-N L<sup>-1</sup> d<sup>-1</sup>, respectively. Statistical fit of the C<sub>50</sub> for NO<sub>3</sub><sup>-</sup> reduction to N<sub>2</sub>O was 14 ± 4 μM (p = 0.08).

### 3.3 Global oceanic N<sub>2</sub>O production

A three-dimensional ocean biogeochemical model incorporating our new data on N<sub>2</sub>O production pathways and their sensitivities to oxygen, was used to estimate marine N<sub>2</sub>O production and oceanic efflux on the global scale. With the formulation of N<sub>2</sub>O yield during nitrification as a function of O<sub>2</sub> concentration (Yield (%) = 0.2 / [O<sub>2</sub>] (μM) + 0.08, Figure 4), global marine N<sub>2</sub>O efflux from nitrification was estimated as 2.2 Tg-N yr<sup>-1</sup>. The contribution

from nitrification is small in the OMZs ( $< 0.05 \text{ Tg-N yr}^{-1}$ ). The uncertainty of  $\text{N}_2\text{O}$  production from nitrification ( $1.1 - 3.3 \text{ Tg-N yr}^{-1}$ , simulation 2 and 3, Table 1) was derived from the parameters' uncertainties of nitrification  $\text{N}_2\text{O}$  yield (Yield =  $(0.2 \pm 0.13) / [\text{O}_2] + (0.08 \pm 0.04)$ ). To estimate the range of  $\text{N}_2\text{O}$  production from denitrification, the varying sensitivities of  $\text{O}_2$  inhibition on  $\text{NO}_2^-$  and  $\text{NO}_3^-$  reduction to  $\text{N}_2\text{O}$  were considered, which were formulated as the rates decreasing by  $1/e$  ( $\sim 36.8\%$ ) for 1.5 (lower boundary), 10 (median) and 20  $\mu\text{M}$  (upper boundary) of  $\text{O}_2$  increase, corresponding to  $\lambda = -0.6667, -0.1$  and  $-0.05$  for Equation (6) (Table 1, simulation 1, 4 and 5). Thus, net  $\text{N}_2\text{O}$  production from denitrification ranged  $0.1 - 2.1 \text{ Tg-N yr}^{-1}$ , with the median estimate of  $0.6 \text{ Tg-N yr}^{-1}$ . Summarizing the above sensitivity analyses, we estimate global oceanic  $\text{N}_2\text{O}$  efflux of  $2.8 \text{ Tg-N yr}^{-1}$  (range  $1.7 - 4.4 \text{ Tg-N yr}^{-1}$ , Table 1), with denitrification across the oxic-anoxic interface in OMZs contributing  $\sim 20\%$  of the total fluxes.

Intense marine  $\text{N}_2\text{O}$  fluxes,  $0.01 - 0.12 \text{ g N m}^{-2} \text{ yr}^{-1}$  (equivalent to  $0.9 - 9 \text{ mmol-N m}^{-2} \text{ yr}^{-1}$ ) occur in the Eastern Tropical Pacific (Figure 7). The high latitude oceans, e.g. the sub-Arctic North Atlantic and the Southern Ocean, are sites with moderate  $\text{N}_2\text{O}$  fluxes. In contrast, the fluxes were negligible in the subtropical gyres in the North and South Pacific, the North Atlantic and South Indian Oceans.

## 4 Discussion

### 4.1 Oxidative vs. reductive $\text{N}_2\text{O}$ production pathways

The Eastern tropical Pacific is regarded as a “hot spot” of  $\text{N}_2\text{O}$  production because of water column  $\text{N}_2\text{O}$  supersaturation near the oxic-anoxic interface. The presence of oxygenated and anoxic environments allow  $\text{N}_2\text{O}$  production via both oxidative and reductive pathways. The availability of  $\text{O}_2$  is an important factor controlling the rate and pathways of  $\text{N}_2\text{O}$  production in OMZs (Codispoti and Christensen, 1985). The application of  $^{15}\text{N}$  tracer

incubation experiments permit the quantitative relationships between O<sub>2</sub> concentration and N<sub>2</sub>O production rates and pathways.

#### 4.1.1 N<sub>2</sub>O production from NH<sub>4</sub><sup>+</sup> oxidation

The production of N<sub>2</sub>O via NH<sub>4</sub><sup>+</sup> oxidation was identified as an important pathway in the OMZ (Cohen and Gordon, 1978). The distribution of rates in the water column of OMZ (Figure 3A) can be explained as follows: (1) In the surface waters (top 30 m), rates of NH<sub>4</sub><sup>+</sup> oxidation to NO<sub>2</sub><sup>-</sup> and N<sub>2</sub>O are minimal, mainly because NH<sub>4</sub><sup>+</sup> oxidation is suppressed by light (Ward, 2005) and phytoplankton competition for NH<sub>4</sub><sup>+</sup>. (2) Within the oxycline above the ODZ, low O<sub>2</sub> conditions stimulated high rates of N<sub>2</sub>O production from NH<sub>4</sub><sup>+</sup> oxidation. This is consistent with O<sub>2</sub> manipulation experiments showing decreased rates of N<sub>2</sub>O production from NH<sub>4</sub><sup>+</sup> oxidation with increasing O<sub>2</sub> concentration (Figure 6A). (3) In the anoxic layer below the oxic-anoxic interface, NH<sub>4</sub><sup>+</sup> oxidation is inhibited, resulting in very low or undetectable rates of N<sub>2</sub>O production from NH<sub>4</sub><sup>+</sup> oxidation. (4) At deeper depths below the ODZ (generally > 500 m), low population density of ammonia oxidizer and low NH<sub>4</sub><sup>+</sup> availability probably limits NH<sub>4</sub><sup>+</sup> oxidation rate (Peng *et al.*, 2016).

In oxygenated waters (> 50 μM O<sub>2</sub>), the measured N<sub>2</sub>O yield of microbial assemblages in ETSP and ETNP (0.003 – 0.06 %) is somewhat similar to those recently measured in cultures of marine ammonia oxidizing bacteria (Frame and Casciotti, 2010) and archaea (Santoro *et al.*, 2011; Löscher *et al.*, 2012; Qin *et al.*, 2017), and is consistent with field measurements outside of OMZ (Yoshida *et al.*, 1989; Grundle *et al.*, 2012). Under suboxic condition ([O<sub>2</sub>] < 5 μM), this and a previous study (Ji *et al.*, 2015) showed N<sub>2</sub>O yield > 1%, which is much higher than any yield measured from archaea but close to bacterial yields (Goreau *et al.*, 1980; Frame and Casciotti, 2010). The empirical relationship of N<sub>2</sub>O yield vs. O<sub>2</sub> concentration presented here showed that outside of OMZ, the N<sub>2</sub>O yield is potentially 2 – 10 fold lower than previously proposed (Nevison *et al.*, 2003), which caused

overestimation of global oceanic N<sub>2</sub>O production from nitrification in some earlier studies (Bianchi *et al.*, 2012; Suntharalingam *et al.*, 2012). Within the OMZ, denitrification is the dominant N<sub>2</sub>O production pathway (see section 4.1.2); thus when estimating N<sub>2</sub>O production via nitrification in OMZ, the error caused by overestimation of N<sub>2</sub>O yield could be negligible.

#### 4.1.2 N<sub>2</sub>O production from NO<sub>2</sub><sup>-</sup> and NO<sub>3</sub><sup>-</sup> reduction

In the anoxic and the peripheral suboxic waters (generally < 10 μM O<sub>2</sub>), our <sup>15</sup>N tracer incubation experiments showed that denitrification is the dominant source of N<sub>2</sub>O production, because rates of N<sub>2</sub>O production from NO<sub>2</sub><sup>-</sup> and NO<sub>3</sub><sup>-</sup> reduction were 10 – 100-fold higher than N<sub>2</sub>O production from NH<sub>4</sub><sup>+</sup> oxidation. Similarly, using N<sub>2</sub>O natural abundance isotopes, a recent study concluded that incomplete denitrification caused N<sub>2</sub>O supersaturation in the Peruvian OMZ (Bourbonnais *et al.*, 2017). Highest rates of N<sub>2</sub>O production from NO<sub>2</sub><sup>-</sup> and NO<sub>3</sub><sup>-</sup> reduction occurred just below the oxic-anoxic interface, where O<sub>2</sub> inhibition of denitrification is relieved and availability of organic matter promotes denitrification. Rates of N<sub>2</sub>O production from NO<sub>2</sub><sup>-</sup> and NO<sub>3</sub><sup>-</sup> reduction were higher at the coastal stations than at the offshore stations (Figure 6). This was likely due to higher organic matter content in the coastal waters resulting from higher particle flux, stimulating the growth of denitrifiers and thus, denitrification (Ward *et al.*, 2008; Babbin *et al.*, 2014). Both NO<sub>2</sub><sup>-</sup> and NO<sub>3</sub><sup>-</sup> are substrates for denitrifiers producing N<sub>2</sub>O. The ratio of rates of the two production pathways is apparently related to the ratio of NO<sub>2</sub><sup>-</sup> and NO<sub>3</sub><sup>-</sup> concentrations (Figure 5). Therefore, high NO<sub>3</sub><sup>-</sup> availability in the water column (Figure S1) probably resulted in higher N<sub>2</sub>O production rates from NO<sub>3</sub><sup>-</sup> than from NO<sub>2</sub><sup>-</sup>. Furthermore, production of N<sub>2</sub>O from NO<sub>3</sub><sup>-</sup> reduction is a series of enzymatic processes, with NO<sub>2</sub><sup>-</sup> as an intermediate, occurring inside denitrifying cells. The exchange of NO<sub>2</sub><sup>-</sup> across cell membranes appears to be limited; and the coupling of NO<sub>3</sub><sup>-</sup> reduction by denitrifiers and NO<sub>2</sub><sup>-</sup> reduction by nitrifiers seems unlikely (Ji *et al.*, 2015;

Trimmer *et al.*, 2016). The reduction of  $\text{NO}_3^-$  to  $\text{NO}_2^-$  ( $0 - 20 \text{ nM-N d}^{-1}$ , data not shown) could lower the  $^{15}\text{N}$  fraction of  $\text{NO}_2^-$  ( $0.4 \mu\text{M}$  added) by  $\sim 5\%$ , which has minimal effect on rate calculation for  $\text{N}_2\text{O}$  production from  $\text{NO}_2^-$ . The production of  $\text{N}_2\text{O}$  from  $\text{NO}_2^-$  reduction, particularly in oxygenated waters, can be attributed to nitrifier-denitrification. Rates of  $\text{NO}_2^-$  reduction to  $\text{N}_2\text{O}$  measured above the oxic-anoxic interface were  $0 - 0.5 \text{ nmol-N L}^{-1} \text{ d}^{-1}$ , similar to rates measured in the peripheral suboxic waters in the ETNP (Trimmer *et al.*, 2016).

Quantitative relationships between  $\text{O}_2$  concentration and rates of  $\text{N}_2\text{O}$  production from  $\text{NO}_2^-$  and  $\text{NO}_3^-$  reduction can be described with half inhibition  $\text{O}_2$  concentration ( $C_{50}$ ). The  $C_{50}$  for  $\text{NO}_2^-$  reduction to  $\text{N}_2\text{O}$  in this study ( $0.6 - 2.4 \mu\text{M}$ ) is somewhat higher than previously reported in the ETSP ( $C_{50} = 0.30 \pm 0.14 \mu\text{M}$ ) (Dalsgaard *et al.*, 2014). By contrast, the  $C_{50}$  for  $\text{NO}_3^-$  reduction to  $\text{N}_2\text{O}$  is 10-fold higher ( $14 \pm 4 \mu\text{M}$ ). Although  $\text{N}_2\text{O}$  production from  $\text{NO}_3^-$  reduction at  $> 7 \mu\text{M O}_2$  was not tested, rates are expected to decrease at higher  $\text{O}_2$  concentrations. In the step-wise denitrification pathway, the enzymes nitrate reductase and nitrite reductase are progressively less oxygen-tolerant (Körner and Zumft, 1989). Thus  $\text{O}_2$  inhibition of denitrifying enzymes should render denitrification as an insignificant pathway in oxygenated waters outside of OMZ.

#### 4.2 Model evaluation for global oceanic $\text{N}_2\text{O}$ flux

With the new quantitative relationships of oxygen and  $\text{N}_2\text{O}$  production from nitrification and denitrification, and sensitivity analyses of nitrification and denitrification parameters, we estimate global oceanic  $\text{N}_2\text{O}$  efflux of  $1.7 - 4.4 \text{ Tg-N yr}^{-1}$ . Production of  $\text{N}_2\text{O}$  outside of OMZs is attributed to nitrification, and denitrification is the dominant pathway in the OMZ. As denitrification in the OMZs contributes 20 % of total oceanic fluxes, denitrification should be regarded as a net  $\text{N}_2\text{O}$  production pathway on a global perspective. Occupying  $< 1\%$  of global ocean volume, the OMZs of the Eastern Tropical Pacific had intense  $\text{N}_2\text{O}$  fluxes,

equivalent to  $0.9 - 9 \text{ mmol-N m}^{-2} \text{ yr}^{-1}$ , which is within the range of previous flux estimates of  $0 - 13 \text{ mmol-N m}^{-2} \text{ yr}^{-1}$  in the ETSP and ETNP (Cohen and Gordon, 1978; Charpentier *et al.*, 2010). The production of  $\text{N}_2\text{O}$  parameterized in this study depends fundamentally on export and remineralization, therefore the relatively lower export production of this model ( $\sim 6 \text{ Pg C yr}^{-1}$ ) resulted lower  $\text{N}_2\text{O}$  production compared to previous studies (Bianchi *et al.*, 2012; Suntharalingam *et al.*, 2012; Battaglia and Joos, 2018). Statistical analysis shows that our median estimate of annual global production,  $2.8 \text{ Tg-N yr}^{-1}$  best reproduces the water column and surface  $\text{N}_2\text{O}$  distribution that are currently available (Figure S2). The oxygen-dependent  $\text{N}_2\text{O}$  production rates presented here could be implemented into higher resolution models in future studies constraining highly variable  $\text{N}_2\text{O}$  fluxes in hypoxic coastal zones (Arevalo-Martinez *et al.*, 2015; Capelle *et al.*, 2018). This study suggests 15 % of the global  $\text{N}_2\text{O}$  emission from oceanic contribution, which is lower than IPCC's estimate of 21 % (Ciais *et al.*, 2013). Thus the global  $\text{N}_2\text{O}$  budget could have a relatively greater contribution from anthropogenic activities on land and coastal environments to global  $\text{N}_2\text{O}$  emissions.

The increased  $\text{N}_2\text{O}$  production rates at low oxygen condition suggests that the ongoing ocean de-oxygenation (thickening and horizontal expansion of ODZs, as well as shoaling of the upper oxycline, Stramma *et al.* (2008) could possibly increase future marine  $\text{N}_2\text{O}$  efflux from the OMZs (Codispoti, 2010). By the end of 21<sup>st</sup> century, it is predicted that the Pacific Ocean will increase the OMZ volume up to 10 % (Cabré *et al.*, 2015), which will likely result in larger volume of suboxic water for net  $\text{N}_2\text{O}$  production from denitrification. Shoaling of the oxycline allows more rapid exchange between  $\text{N}_2\text{O}$ -supersaturated water and the atmosphere. It is still an open question whether the global oceanic  $\text{N}_2\text{O}$  flux will increase with the ongoing ocean warming. On one hand, warming of the surface ocean lowers  $\text{N}_2\text{O}$  solubility, leading to less  $\text{N}_2\text{O}$  retained in seawater during production, and thus to increased oceanic  $\text{N}_2\text{O}$  emissions. On the other hand, the global oceanic primary production would

decrease and cause lower water column remineralization and thus, lower N<sub>2</sub>O production (Martinez-Rey *et al.*, 2015; Landolfi *et al.*, 2017). Experimental approaches to quantify the effect of organic matter availability on N<sub>2</sub>O production rates and pathways could facilitate predicting future oceanic N<sub>2</sub>O emissions.

## 5 Conclusion

In the vicinity of water column oxic-anoxic interface within the OMZs of the Eastern tropical Pacific, active N<sub>2</sub>O production was measured via oxidative (NH<sub>4</sub><sup>+</sup> oxidation) and reductive pathways (NO<sub>2</sub><sup>-</sup> and NO<sub>3</sub><sup>-</sup> reduction). Production of N<sub>2</sub>O from NH<sub>4</sub><sup>+</sup> oxidation occurred in the oxygenated waters, with higher rates at lower in situ oxygen concentrations. The N<sub>2</sub>O yield during nitrification increases with decreasing oxygen concentrations; and the field measurements of N<sub>2</sub>O yield were much lower (by 2 – 10-fold) than those from culture experiments. Reduction of NO<sub>2</sub><sup>-</sup> and NO<sub>3</sub><sup>-</sup> to N<sub>2</sub>O mainly occurred in the anoxic layer and suboxic zones ([O<sub>2</sub>] < 5 μM) above the anoxic layer. Production of N<sub>2</sub>O via the reductive pathways had much higher rates than that of oxidative pathway. Increasing oxygen concentrations (up to 7 μM) significantly inhibited NO<sub>2</sub><sup>-</sup> reduction to N<sub>2</sub>O; however, NO<sub>3</sub><sup>-</sup> reduction to N<sub>2</sub>O was not effectively inhibited. The relative abundance of water column NO<sub>3</sub><sup>-</sup> and NO<sub>2</sub><sup>-</sup> positively correlated with relative rates of N<sub>2</sub>O production from respective substrates. In all, denitrification, particularly NO<sub>3</sub><sup>-</sup> reduction is the dominating N<sub>2</sub>O production pathway in the OMZ and adjacent suboxic waters.

We quantified the effects of oxygen concentration on N<sub>2</sub>O production from both oxidative and reductive pathways, and implemented into a global ocean model and estimated global oceanic N<sub>2</sub>O flux of 1.7 – 4.4 Tg-N yr<sup>-1</sup>. Although OMZs occupy a small fraction of ocean volume, high rates of N<sub>2</sub>O production from denitrification result in OMZs contributed 20 % of oceanic N<sub>2</sub>O source. Thus, denitrification should be viewed as a net N<sub>2</sub>O production pathway on a global perspective.

## Acknowledgments

The authors would like to thank B. Widner and P. Bernhardt for providing seawater nutrient analysis; G. Alarcón for the PPS operations and the STOX sensor data on R/V Atlantis; M. Blum for the PPS operations on R/V Ronald H. Brown and M. Mulholland as chief scientist on R/V Atlantis and Ronald H. Brown. During laboratory analysis, S. Oleynik provided valuable assistance. This research was supported by US-NSF grants OCE-1356043 to B. B. Ward, A. Jayakumar and M. Mulholland. Erik Buitenhuis and Parvadha Suntharalingam acknowledge support from the EU H2020 CRESCENDO project. The authors declare no competing financial interests. The manuscript is prepared to comply with AGU data policy. The data reported in this study can be found in the supplementary dataset.

## References

- Arevalo-Martinez, D. L., Kock, A., Loscher, C. R., Schmitz, R. A., & Bange, H. W. (2015). Massive nitrous oxide emissions from the tropical south pacific ocean, *Nature Geosciences*, 8(7), 530-533. <https://doi.org/10.1038/ngeo2469>
- Babbin, A. R., Keil, R. G., Devol, A. H., & Ward, B. B. (2014). Organic matter stoichiometry, flux, and oxygen control nitrogen loss in the ocean, *Science*, 344(6182), 406-408. <https://doi.org/10.1126/science.1248364>
- Babbin, A. R., Bianchi, D., Jayakumar, A., & Ward, B. B. (2015). Rapid nitrous oxide cycling in the suboxic ocean, *Science*, 348(6239), 1127-1129. <https://doi.org/10.1126/science.aaa8380>
- Battaglia, G., & Joos, F. (2018). Marine n<sub>2</sub>o emissions from nitrification and denitrification constrained by modern observations and projected in multimillennial global warming simulations, *Global Biogeochemical Cycles*, 32(1), 92-121. doi:10.1002/2017GB005671
- Bianchi, D., Dunne, J. P., Sarmiento, J. L., & Galbraith, E. D. (2012). Data-based estimates of suboxia, denitrification, and n<sub>2</sub>o production in the ocean and their sensitivities to dissolved o<sub>2</sub>, *Global Biogeochemical Cycles*, 26(2), 6550–6555. <https://doi.org/10.1029/2011GB004209>
- Bisson, K. M., Siegel, D. A., DeVries, T., Cael, B. B., & Buesseler, K. O. (2018). How dataset characteristics influence ocean carbon export models, *Global Biogeochemical Cycles*, 0(32). doi:10.1029/2018GB005934
- Blasing, T. J. (2016). Recent greenhouse gas concentrations, Environmental System Science Data Infrastructure for a Virtual Ecosystem; Carbon Dioxide Information Analysis Center (CDIAC), Oak Ridge National Laboratory (ORNL), Oak Ridge, TN (United States), United States. 10.3334/CDIAC/atg.032
- Bourbonnais, A., Letscher, R. T., Bange, H. W., Échevin, V., Larkum, J., Mohn, J., et al. (2017). N<sub>2</sub>o production and consumption from stable isotopic and concentration data in the peruvian coastal upwelling system, *Global Biogeochemical Cycles*, 31(4), 678-698. <https://doi.org/10.1002/2016GB005567>
- Buitenhuis, E. T., Suntharalingam, P., & Le Quéré, C. (2018). Constraints on global oceanic emissions of n<sub>2</sub>o from observations and models, *Biogeosciences*, 15(7), 2161-2175.
- Cabré, A., Marinov, I., Bernardello, R., & Bianchi, D. (2015). Oxygen minimum zones in the tropical pacific across cmip5 models: Mean state differences and climate change trends, *Biogeosciences*, 12(18), 5429-5454.
- Capelle, D. W., Hawley, A. K., Hallam, S. J., & Tortell, P. D. (2018). A multi-year time-series of n<sub>2</sub>o dynamics in a seasonally anoxic fjord: Saanich inlet, british columbia, *Limnology and Oceanography*, 63(2), 524-539. doi:10.1002/lo.10645
- Charpentier, J., Fariás, L., & Pizarro, O. (2010). Nitrous oxide fluxes in the central and eastern south pacific, *Global Biogeochemical Cycles*, 24(3). <https://doi.org/10.1029/2008gb003388>

Ciais, P., C. Sabine, G. Bala, L. Bopp, V. Brovkin, J. Canadell, et al. (2013), Carbon and other biogeochemical cycles, 465–570 pp, Cambridge, United Kingdom and New York, NY, USA.  
<https://doi.org/10.1017/CBO9781107415324.015>.

Codispoti, L. A. (2010). Interesting times for marine  $\text{N}_2\text{O}$ , *Science*, 327(5971), 1339-1340.  
<https://doi.org/10.1126/science.1184945>

Codispoti, L. A., & Christensen, J. P. (1985). Nitrification, denitrification and nitrous oxide cycling in the eastern tropical south pacific ocean, *Marine Chemistry*, 16(4), 277-300. [https://doi.org/10.1016/0304-4203\(85\)90051-9](https://doi.org/10.1016/0304-4203(85)90051-9)

Codispoti, L. A., Brandes, J. A., Christensen, J. P., Devol, A. H., Naqvi, S. W. A., Paerl, H. W., & Yoshinari, T. (2001). The oceanic fixed nitrogen and nitrous oxide budgets: Moving targets as we enter the anthropocene?, *Scientia Marina*, 65(S2), 85-105.

Cohen, Y., & Gordon, L. I. (1978). Nitrous oxide in the oxygen minimum of the eastern tropical north pacific: Evidence for its consumption during denitrification and possible mechanisms for its production, *Deep-Sea Research*, 25(6), 509-524. [https://doi.org/10.1016/0146-6291\(78\)90640-9](https://doi.org/10.1016/0146-6291(78)90640-9)

Dalsgaard, T., Stewart, F. J., Thamdrup, B., De Brabandere, L., Revsbech, N. P., Ulloa, O., et al. (2014). Oxygen at nanomolar levels reversibly suppresses process rates and gene expression in anammox and denitrification in the oxygen minimum zone off northern chile, *mBio*, 5(6). <https://doi.org/10.1128/mBio.01966-14>

Elkins, J. W., Steven C. Wofsy, Michael B. McElroy, Charles E. Kolb, & Kaplan, W. A. (1978). Aquatic sources and sinks for nitrous oxide, *Nature*, 275(5681), 602-606. <https://doi.org/10.1038/275602a0>

Frame, C. H., & Casciotti, K. L. (2010). Biogeochemical controls and isotopic signatures of nitrous oxide production by a marine ammonia-oxidizing bacterium, *Biogeosciences*, 7(9), 2695-2709.  
<https://doi.org/10.5194/bg-7-2695-2010>

Freing, A., Wallace, D. W., & Bange, H. W. (2012). Global oceanic production of nitrous oxide, *Philosophical transactions of the Royal Society of London. Series B, Biological sciences*, 367(1593), 1245-1255.  
<https://doi.org/10.1098/rstb.2011.0360>

Freing, A., Wallace, D. W. R., Tanhua, T., Walter, S., & Bange, H. W. (2009). North atlantic production of nitrous oxide in the context of changing atmospheric levels, *Global Biogeochemical Cycles*, 23(4).  
doi:10.1029/2009GB003472

Garcia, H. E., & Gordon, L. I. (1992). Oxygen solubility in seawater: Better fitting equations, *Limnology and Oceanography*, 37(6), 1307-1312.

Goreau, T. J., Kaplan, W. A., Wofsy, S. C., McElroy, M. B., Valois, F. W., & Watson, S. W. (1980). Production of  $\text{NO}_2^-$  and  $\text{N}_2\text{O}$  by nitrifying bacteria at reduced concentrations of oxygen, *Applied and Environmental Microbiology*, 40(3), 526-532.

Grundle, D. S., Maranger, R., & Juniper, S. K. (2012). Upper water column nitrous oxide distributions in the northeast subarctic pacific ocean, *Atmosphere-Ocean*, 50(4), 475-486. 10.1080/07055900.2012.727779

Hansen, H. P., & Koroleff, F. (1999), *Determination of nutrients*, Wiley-VCH Verlag GmbH, Wiley-VCH Verlag GmbH, Weinheim, Germany.

Holmes, R. M., Aminot, A., Kerouel, R., Hooker, B. A., & Peterson, B. J. (1999). A simple and precise method for measuring ammonium in marine and freshwater ecosystems, *Canadian Journal of Fisheries and Aquatic Sciences*(56), 1801-1808. <https://doi.org/10.1139/f99-128> (1999)

Ji, Q., Babbin, A. R., Jayakumar, A., Oleynik, S., & Ward, B. B. (2015). Nitrous oxide production by nitrification and denitrification in the eastern tropical south pacific oxygen minimum zone, *Geophysical Research Letters*, 42(24), 10,755-10,764. <https://doi.org/10.1002/2015GL066853>

Kock, A., & Bange, H. W. (2015). Counting the ocean's greenhouse gas emissions, *Eos*(96), 10-13. <https://doi.org/10.1029/2015EO023665>

Körner, H., & Zumft, W. G. (1989). Expression of denitrification enzymes in response to the dissolved oxygen level and respiratory substrate in continuous culture of *pseudomonas stutzeri*, *Applied and Environmental Microbiology*, 55(7), 1670-1676.

Landolfi, A., Somes, C. J., Koeve, W., Zamora, L. M., & Oschlies, A. (2017). Oceanic nitrogen cycling and n<sub>2</sub>O flux perturbations in the anthropocene, *Global Biogeochemical Cycles*, 31(8), 1236-1255. doi:10.1002/2017GB005633

Law, C. S., & Owens, N. J. P. (1990). Significant flux of atmospheric nitrous oxide from the northwest indian ocean, *Nature*, 346(6287), 826-828. <https://doi.org/10.1038/346826a0>

Le Quéré, C., Buitenhuis, E. T., Moriarty, R., Alvain, S., Aumont, O., Bopp, L., et al. (2016). Role of zooplankton dynamics for southern ocean phytoplankton biomass and global biogeochemical cycles, *Biogeosciences*, 13(14), 4111-4133. <https://doi.org/10.5194/bg-13-4111-2016>

Löscher, C. R., Kock, A., Könneke, M., LaRoche, J., Bange, H. W., & Schmitz, R. A. (2012). Production of oceanic nitrous oxide by ammonia-oxidizing archaea, *Biogeosciences*, 9(7), 2419-2429. <https://doi.org/10.5194/bg-9-2419-2012>

Madec, G., Delecluse, P., Imbard, M., & Lévy, C. (1998). Opa 8.1 ocean general circulation model reference manual, notes pole model, edited by I. P. S. L. d. S. d. I. E. Global, p. 91, Laboratoire d'Océanographie DYnamique et de Climatologie.

Martinez-Rey, J., Bopp, L., Gehlen, M., Tagliabue, A., & Gruber, N. (2015). Projections of oceanic n<sub>2</sub>O emissions in the 21st century using the ipsl earth system model, *Biogeosciences*, 12(13), 4133-4148. 10.5194/bg-12-4133-2015

McIlvin, M. R., & Altabet, M. A. (2005). Chemical conversion of nitrate and nitrite to nitrous oxide for nitrogen and oxygen isotopic analysis in freshwater and seawater, *Analytical Chemistry*, 77(17), 5589-5595.

Nevison, C., Butler, J. H., & Elkins, J. W. (2003). Global distribution of n<sub>2</sub>O and the δn<sub>2</sub>O-aou yield in the subsurface ocean, *Global Biogeochemical Cycles*, 17(4). <https://doi.org/10.1029/2003GB002068>

Peng, X., Fuchsman, C. A., Jayakumar, A., Warner, M. J., Devol, A. H., & Ward, B. B. (2016). Revisiting nitrification in the eastern tropical south pacific: A focus on controls, *Journal of Geophysical Research: Oceans*, 121(3), 1667-1684. 10.1002/2015JC011455

Poth, M., & Focht, D. D. (1985). (15)n kinetic analysis of n(2)o production by *nitrosomonas europaea*: An examination of nitrifier denitrification, *Applied and Environmental Microbiology*, 49(5), 1134-1141.

Prather, M. J., Holmes, C. D., & Hsu, J. (2012). Reactive greenhouse gas scenarios: Systematic exploration of uncertainties and the role of atmospheric chemistry, *Geophysical Research Letters*, 39(9). <https://doi.org/10.1029/2012GL051440>

Qin, W., Meinhardt, K. A., Moffett, J. W., Devol, A. H., Virginia Armbrust, E., Ingalls, A. E., & Stahl, D. A. (2017). Influence of oxygen availability on the activities of ammonia-oxidizing archaea, *Environmental Microbiology Reports*, 9(3), 250-256. <https://doi.org/10.1111/1758-2229.12525>

Ravishankara, A., Daniel, J. S., & Portmann, R. W. (2009). Nitrous oxide (n<sub>2</sub>O): The dominant ozone-depleting substance emitted in the 21st century, *Science*, 326(5949), 123-125.

Revsbech, N. P., Larsen, L. H., Gundersen, J., Dalsgaard, T., Ulloa, O., & Thamdrup, B. (2009). Determination of ultra-low oxygen concentrations in oxygen minimum zones by the stox sensor, *Limnology and Oceanography Methods*, 7, 371-381.

Santoro, A. E., Buchwald, C., McIlvin, M. R., & Casciotti, K. L. (2011). Isotopic signature of n(2)o produced by marine ammonia-oxidizing archaea, *Science*, 333(6047), 1282-1285. <https://doi.org/10.1126/science.1208239>

- Siegel, D. A., Buesseler, K. O., Doney, S. C., Sailley, S. F., Behrenfeld, M. J., & Boyd, P. W. (2014). Global assessment of ocean carbon export by combining satellite observations and food-web models, *Global Biogeochemical Cycles*, 28(3), 181-196. doi:10.1002/2013GB004743
- Stramma, L., Johnson, G. C., Sprintall, J., & Mohrholz, V. (2008). Expanding oxygen-minimum zones in the tropical oceans, *Science*, 320(5876), 655-658. <https://doi.org/10.1126/science.1153847>
- Suntharalingam, P., Buitenhuis, E., Le Quéré, C., Dentener, F., Nevison, C., Butler, J. H., et al. (2012). Quantifying the impact of anthropogenic nitrogen deposition on oceanic nitrous oxide, *Geophysical Research Letters*, 39(7). <https://doi.org/10.1029/2011GL050778>
- Takahashi, T., Broecker, W. S., & Langer, S. (1985). Redfield ratio based on chemical data from isopycnal surfaces, *Journal of Geophysical Research: Oceans*, 90(C4), 6907-6924. <https://doi.org/10.1029/JC090iC04p06907>
- Trimmer, M., Chronopoulou, P.-M., Maanoja, S. T., Upstill-Goddard, R. C., Kitidis, V., & Purdy, K. J. (2016). Nitrous oxide as a function of oxygen and archaeal gene abundance in the north pacific, *Nature Communications*, 7, 13451. <https://doi.org/10.1038/ncomms13451>
- UNESCO (1994), Protocols for the joint global ocean flux study (jgofs) core measurements, edited by I. O. Commission, United Nations Educational, Scientific and Cultural Organization.
- Wanninkhof, R. (1992). Relationship between wind speed and gas exchange over the ocean, *Journal of Geophysical Research: Oceans*, 97(C5), 7373-7382. <https://doi.org/10.1029/92JC00188>
- Ward, B. B. (2005). Temporal variability in nitrification rates and related biogeochemical factors in monterey bay, california, USA, *Marine Ecology Progress Series*, 292, 97-109. <https://doi.org/10.3354/meps292097>
- Ward, B. B., Tuit, C. B., Jayakumar, A., Rich, J. J., Moffett, J., & Naqvi, S. W. A. (2008). Organic carbon, and not copper, controls denitrification in oxygen minimum zones of the ocean, *Deep-Sea Research Part I*, 55(12), 1672-1683. <https://doi.org/10.1016/j.dsr.2008.07.005>
- Weiss, R. F., & Price, B. A. (1980). Nitrous oxide solubility in water and seawater, *Marine Chemistry*, 8(4), 347-359. [https://doi.org/10.1016/0304-4203\(80\)90024-9](https://doi.org/10.1016/0304-4203(80)90024-9)
- Wilson, S. T., del Valle, D. A., Segura-Noguera, M., & Karl, D. M. (2014). A role for nitrite in the production of nitrous oxide in the lower euphotic zone of the oligotrophic north pacific ocean, *Deep-Sea Research Part I*, 85, 47-55. <https://doi.org/10.1016/j.dsr.2013.11.008>
- Yoshida, N., Morimoto, H., Hirano, M., Koike, I., Matsuo, S., Wada, E., et al. (1989). Nitrification rates and  $^{15}\text{n}$  abundances of  $\text{N}_2\text{O}$  and  $\text{NO}_3^-$  in the western north pacific, *Nature*, 342(6252), 895-897. 10.1038/342895a0

**Table 1.** Sensitivity analysis of annual global oceanic N<sub>2</sub>O production from nitrification and denitrification. Median production was calculated based on median parameterizations for both nitrification and denitrification (simulation 1). The uncertainties for N<sub>2</sub>O production from nitrification and denitrification were derived from simulations 2 and 3, and simulation 4 and 5, respectively.

Simulation number	Nitrification yield $J_1 = [a / [O_2] (\mu M) + b]$	Denitrification $f(O_2) = \exp(\lambda (O_2 (\mu M) - 1)$	N <sub>2</sub> O production from nitrification (Tg N yr <sup>-1</sup> )	N <sub>2</sub> O production from denitrification (Tg N yr <sup>-1</sup> )	Annual N <sub>2</sub> O production (Tg N)
1	$a = 0.2, b = 0.08$	$\lambda = -0.1$ ( <i>e</i> -folding [O <sub>2</sub> ] = 10 μM)	2.2	0.6	2.8
2	$a = 0.07, b = 0.04$	$\lambda = -0.1$ ( <i>e</i> -folding [O <sub>2</sub> ] = 10 μM)	1.1	0.6	1.7
3	$a = 0.33, b = 0.12$	$\lambda = -0.1$ ( <i>e</i> -folding [O <sub>2</sub> ] = 10 μM)	3.3	0.6	3.9
4	$a = 0.2, b = 0.08$	$\lambda = -0.6667$ ( <i>e</i> -folding [O <sub>2</sub> ] = 1.5 μM)	2.2	0.1	2.3
5	$a = 0.2, b = 0.08$	$\lambda = -0.05$ ( <i>e</i> -folding [O <sub>2</sub> ] = 20 μM)	2.2	2.1	4.3

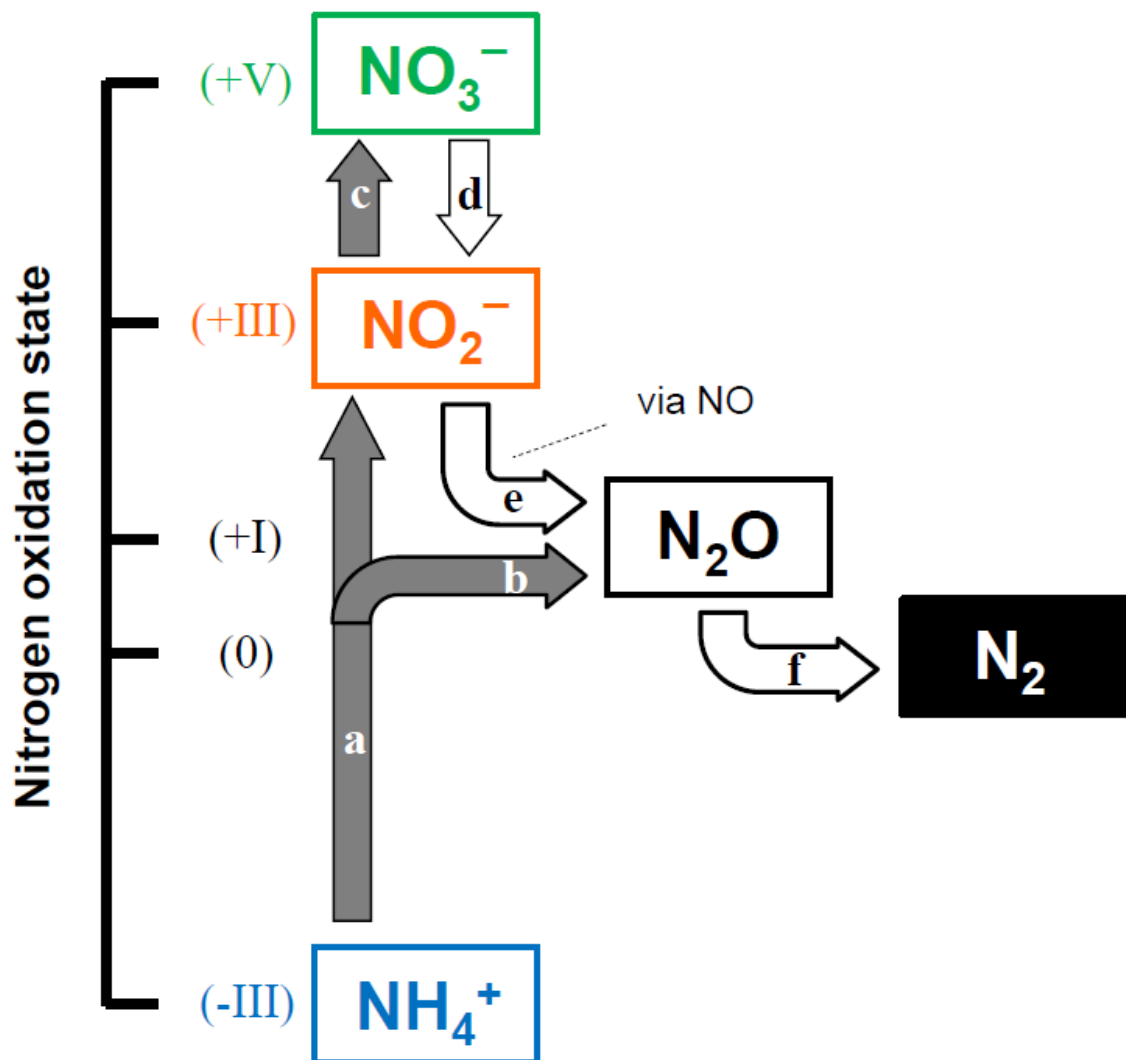


**Figure 1.** Nitrogen transformations related to  $\text{N}_2\text{O}$  production and consumption in marine environments. (a) Ammonium ( $\text{NH}_4^+$ ) oxidation to nitrite ( $\text{NO}_2^-$ ). (b)  $\text{NH}_4^+$  oxidation to  $\text{N}_2\text{O}$ . (c)  $\text{NO}_2^-$  oxidation to nitrate ( $\text{NO}_3^-$ ). (d)  $\text{NO}_3^-$  reduction to  $\text{NO}_2^-$ . (e)  $\text{NO}_2^-$  reduction to  $\text{N}_2\text{O}$  via nitric oxide (NO). (f)  $\text{N}_2\text{O}$  reduction to  $\text{N}_2$ . Filled arrows (reaction (a), (b) and (c)) represent oxidative pathways, requiring molecular oxygen as terminal electron acceptor. Open arrows (reaction (d), (e) and (f)) represent reductive pathways requiring organic matter as the electron donor. In the main text,  $\text{N}_2\text{O}$  production from nitrification includes pathways (b) and (a) coupled with (e);  $\text{N}_2\text{O}$  production from denitrification includes pathways (e) and (d) coupled with (e).

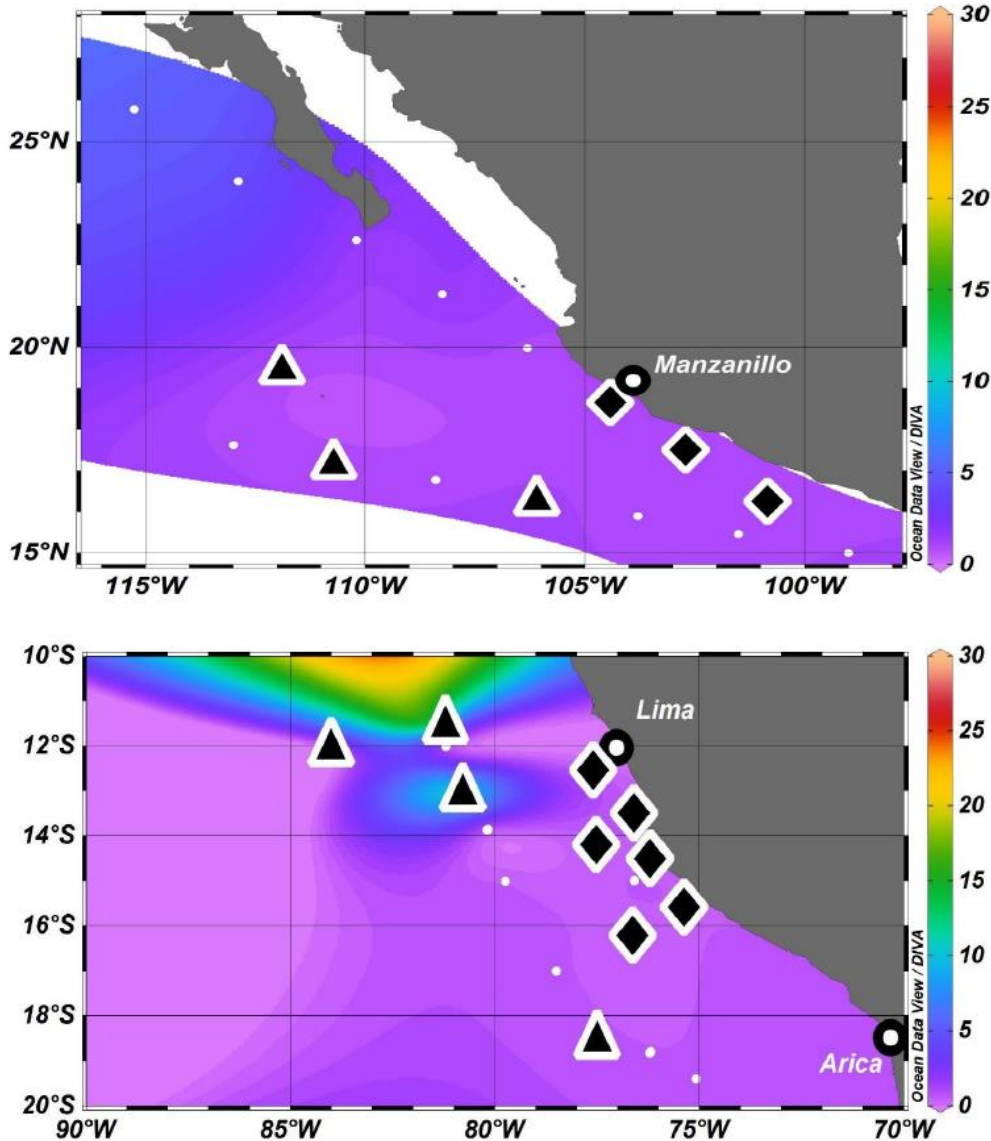


**Figure 2.** Sampling locations during cruises in 2016 ETNP (upper panel) and 2015 ETSP (lower panel). Comprehensive measurements of nitrous oxide production were performed at stations representing coastal environment (diamonds) and open-ocean environment (triangles). High resolution oxygen profiles were obtained at both comprehensive stations and transect stations (dots). Color map shows minimum dissolved oxygen concentration ( $\mu\text{mol L}^{-1}$ ) within the upper 1000 m water column.

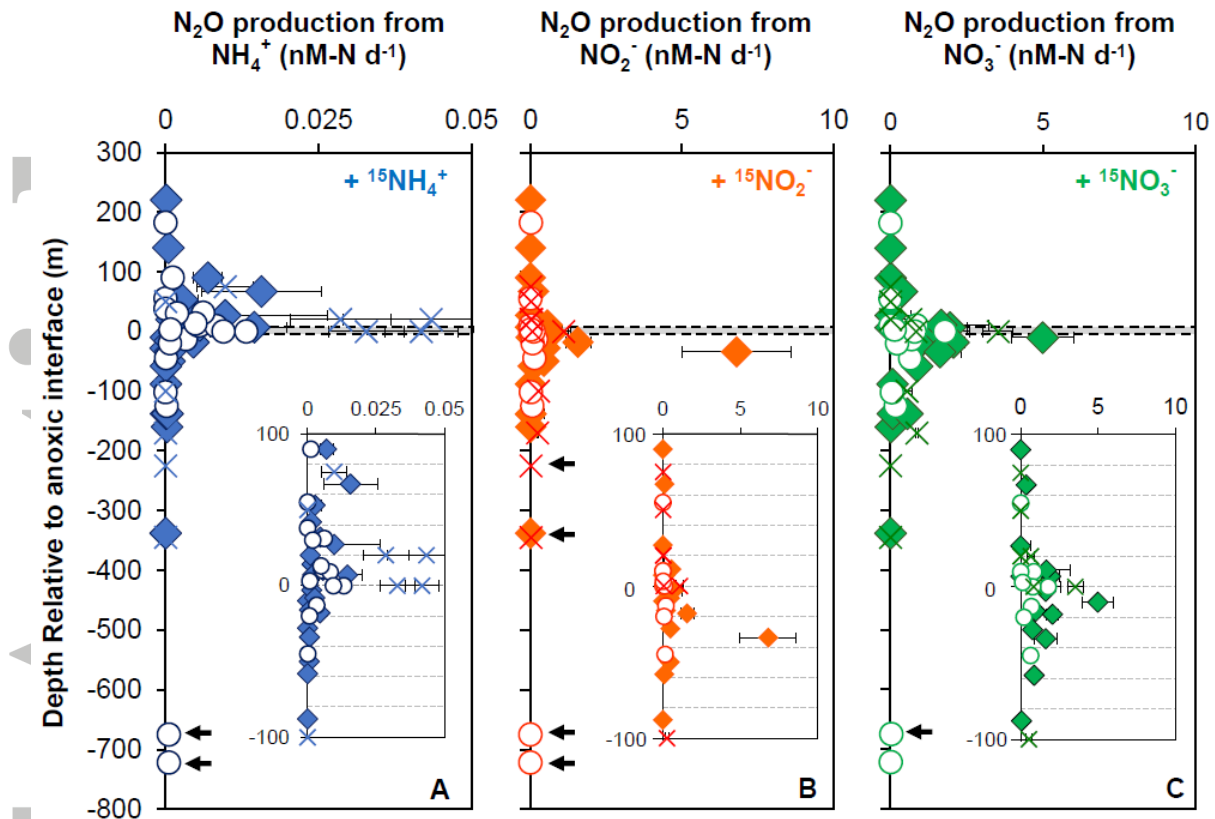


**Figure 3.** Rates of  $\text{N}_2\text{O}$  production from  $\text{NH}_4^+$  oxidation (A),  $\text{NO}_2^-$  reduction (B) and  $\text{NO}_3^-$  reduction (C) at depths relative to the oxic-anoxic interface (shaded line) during cruises in 2013 ETSP (crosses), 2015 ETSP (filled diamonds) and 2016 ETNP (open circles). Arrows represent significant ( $p < 0.05$ , see methods) production rates at depth  $\geq 200$  m below oxic-anoxic interface. Inset:  $\text{N}_2\text{O}$  production from  $\text{NH}_4^+$  oxidation (A),  $\text{NO}_2^-$  reduction (B) and  $\text{NO}_3^-$  reduction (C) within  $\pm 100$  m of the oxic-anoxic interface. Error bar represents standard deviation of rates derived from a linear fit to three time points measured in duplicate ( $n = 5$ ).

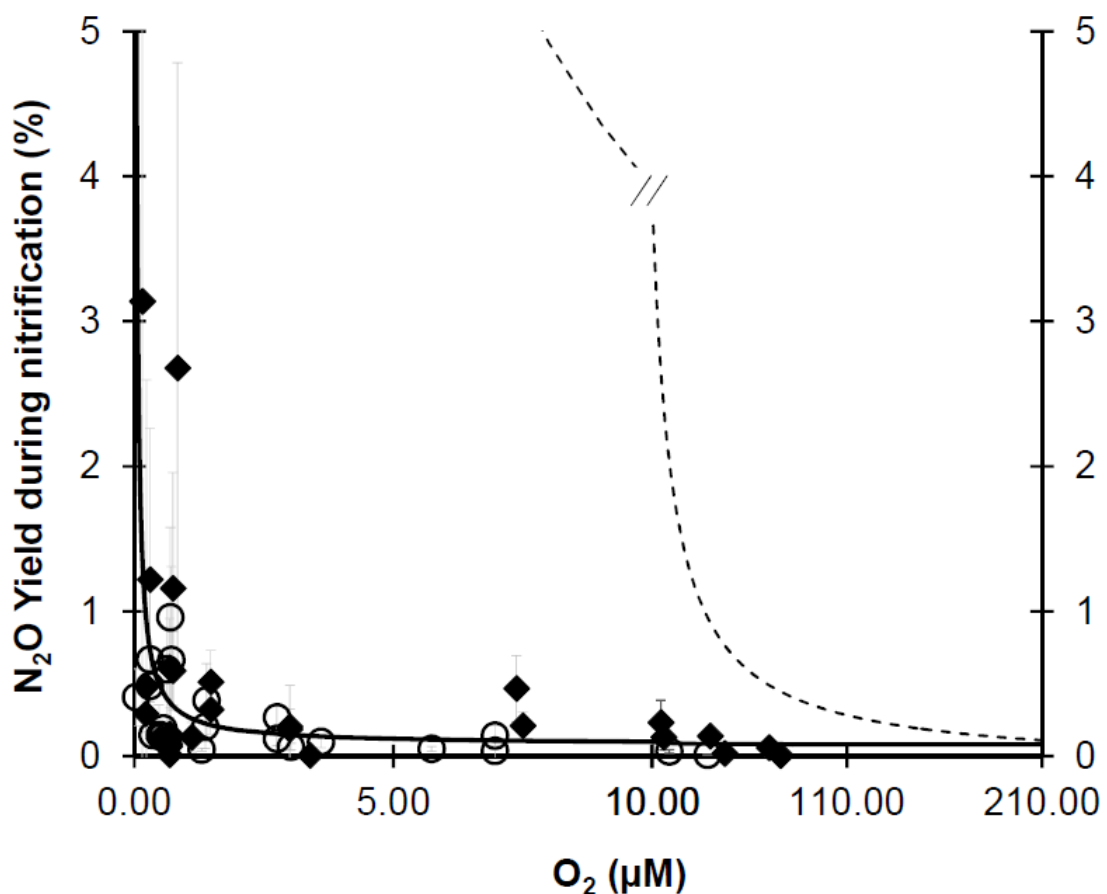


**Figure 4.**  $N_2O$  yield (%) during nitrification, the molar nitrogen ratio of  $N_2O$  production to  $NO_2^-$  production during  $NH_4^+$  oxidation, measured at a range of  $O_2$  concentrations. Data are from cruises in 2015 ETSP (filled diamonds) and 2016 ETNP (open circles) and compared to the  $N_2O$  yield vs. oxygen relationship based on the bacterial culture work (Goreau *et al.*, 1980; Nevison *et al.*, 2003) (dashed line) and the empirical fit in this study (solid line, Yield (%) =  $0.2/[O_2]$  ( $\mu M$ ) + 0.08).

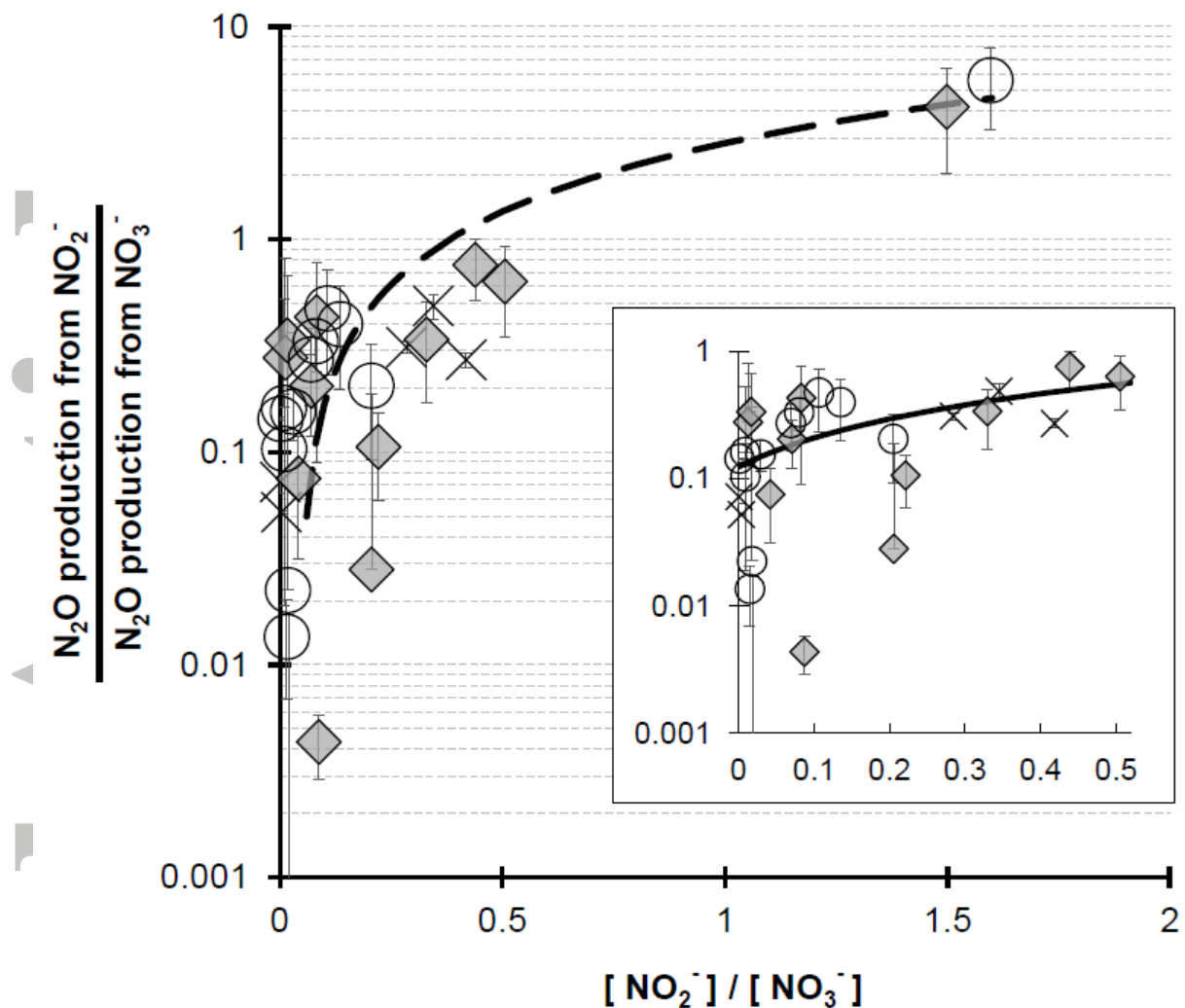


**Figure 5.** The ratio of  $\text{N}_2\text{O}$  production rates from  $\text{NO}_2^-$  and that from  $\text{NO}_3^-$  plotted against ratio of  $\text{NO}_2^-$  and  $\text{NO}_3^-$  concentrations during incubation experiments. Only significant production rates are plotted. Data are from cruises of 2013 ETSP (cross), 2015 ETSP (filled diamonds) and 2016 ETNP (circles). Linear regressions were statistically significant for data with  $\text{NO}_2^-$  and  $\text{NO}_3^-$  concentration ratios below 0.5 (solid line, inset) and below 1.6 (dashed line). Curvature of linear regression was due to logarithmic scale on y-axis. Inset: Plotted data with  $\text{NO}_2^-$  and  $\text{NO}_3^-$  concentration ratio < 0.5.

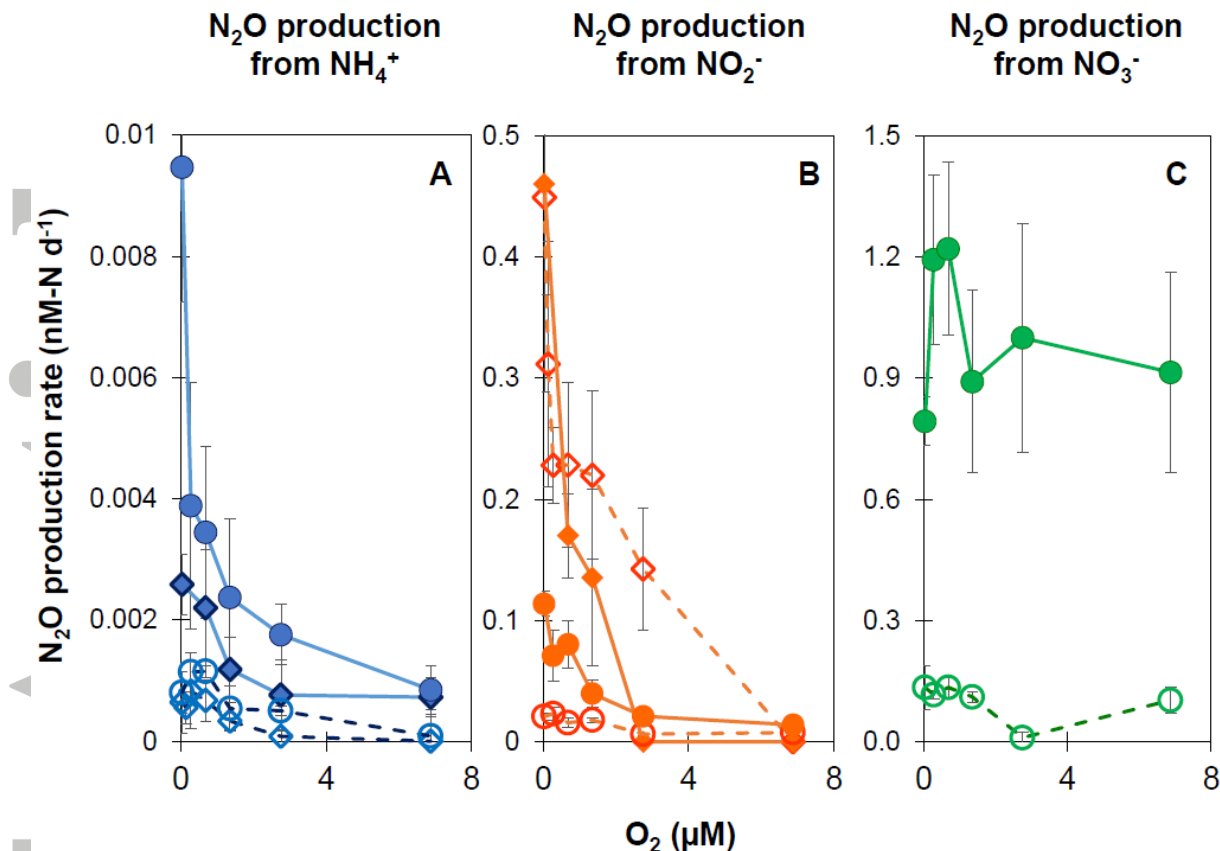


**Figure 6.** Rates of  $\text{N}_2\text{O}$  production from  $\text{NH}_4^+$  oxidation (A),  $\text{NO}_2^-$  reduction (B) and  $\text{NO}_3^-$  reduction (C) under manipulated oxygen concentrations during cruises in 2015 ETSP (diamonds) and 2016 ETNP (circles). Measurements were performed at stations representing coastal environment (filled symbols) and open-ocean environment (open symbols). The *in situ* oxygen concentrations at the time of sampling was  $< 0.1 \mu\text{M}$ . Standard deviation of rates derived from a linear fit to three time points measured in duplicate ( $n = 5$ ).

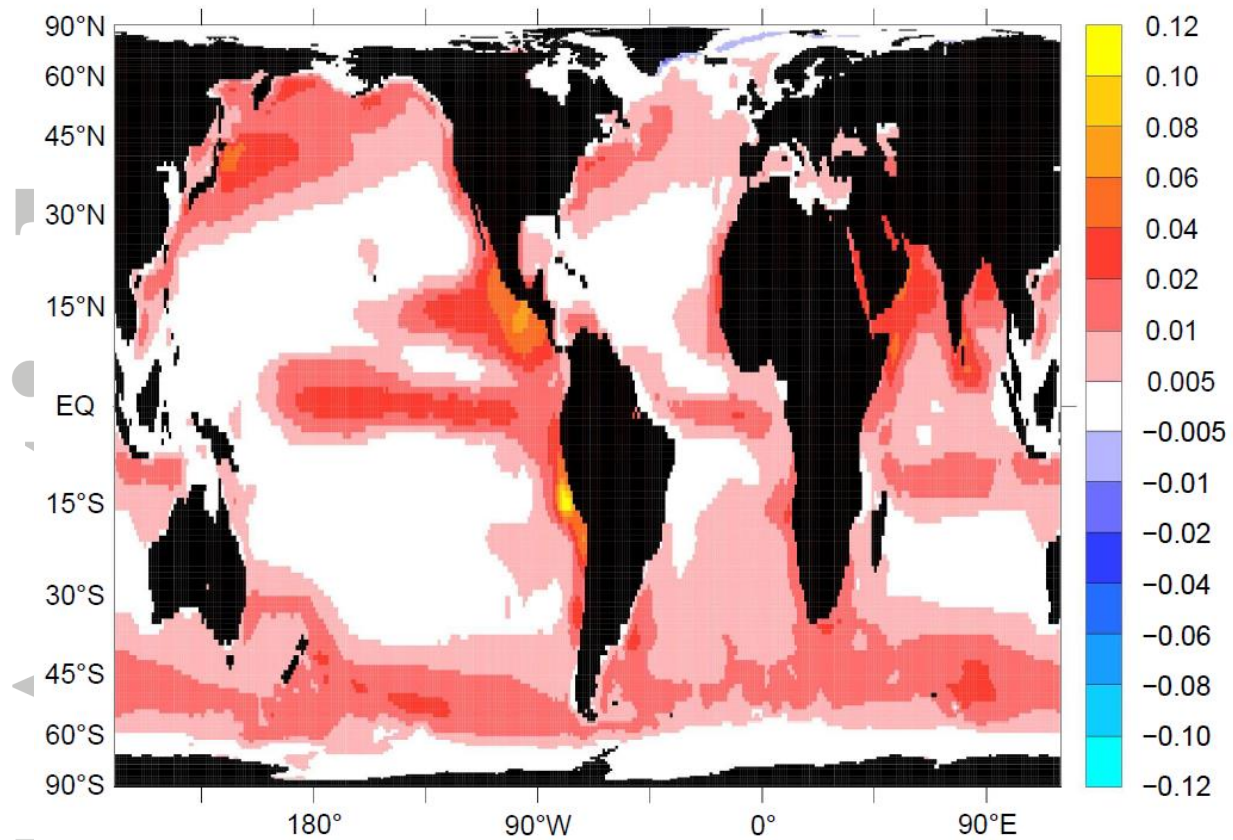


**Figure 7.** Global ocean  $\text{N}_2\text{O}$  flux ( $\text{g N m}^{-2} \text{ yr}^{-1}$ , color bar on right) determined by a model simulation. Positive values indicate net flux from the ocean to the atmosphere. Simulation were performed with nitrification parameterization from this study ( $\text{N}_2\text{O}$  yield (%)) =  $0.2/\text{[O}_2\text{]}+0.08$ ), and denitrification parameterization of e-folding  $[\text{O}_2] = 10 \mu\text{M}$ . The result of global oceanic net  $\text{N}_2\text{O}$  production is  $2.8 \times 10^{12} \text{ g N yr}^{-1}$ .